PROTEINS: Structure, Function, and Genetics 18:49–62 (1994)

X-Ray Structures of Fragments From Binding and Nonbinding Versions of a Humanized Anti-CD18 Antibody: Structural Indications of the Key Role of V_H Residues 59 to 65

Charles Eigenbrot,[1] Tania Gonzalez,[1] Julie Mayeda,[2] Paul Carter,[2] Winifred Werther,[3] Timothy Hotaling,[4] Judy Fox,[4] and Jeremy Kessler[1]

Departments of [1]Protein Engineering, [2]Cell Genetics, [3]Immunology, and [4]Pharmacology, Genentech, Inc., South San Francisco, California 94080-4990

ABSTRACT **X-ray crystal structures of fragments from two different humanized anti-CD18 antibodies are reported. The Fv fragment of the nonbinding version has been refined in space group C2 with $a=64.2$ Å, $b=61.3$ Å, $c=51.8$ Å, and $\beta=99°$ to an *R*-value of 18.0% at 1.9 Å, and the Fab fragment of the tight-binding version has been refined in space group *P*3 with $a=101.$ Å and $c=45.5$ Å to an *R*-value of 17.8% at 3.0 Å resolution. The very large difference in their binding affinity (>1000-fold) is attributed to large and local structural differences in the C-terminal part of CDR-H2, and from this we conclude there is direct contact between this region and antigen when they combine. X-ray structures of antibody–antigen complexes available in the literature have yet to show this part of CDR-H2 in contact with antigen, despite its hypervariable sequence. Implications of this result for antibody humanization are discussed.**

Key words: protein, mutation, Fab, Fv, complementarity determining region, hypervariability, integrin

INTRODUCTION

The tight and highly specific binding characteristic of antibodies is afforded by the combination of six loops (CDRs) forming a surface atop the variable region. Complexes between small molecular haptens or peptides and antibodies often do not involve all 6 CDRs, but most X-ray structures of antibodies complexes with a protein antigen show all six CDRs involved in direct interaction with antigen.[1] The contribution to antigen binding (gauged by counting contacts) is generally not distributed equally among the CDRs, nor do they contribute in a consistent rank order.[2] In short, any CDR can be important. However, as discussed by Davies et al.[2] and more recently by Wilson and Stanfield,[3] the heavy chain makes more contacts than the light chain, and this is especially so for small antigens.

The available structural information on protein–antibody complexes is somewhat at odds with the observed sequence hypervariability of the antigen-binding loop regions. Kabat and co-workers have shown that CDRs are characterized by high sequence variability from one antibody to the next,[4] but the number of antibody residues found by direct evidence to be part of an antibody–antigen interface or to provide key constraints on the presentation of such residues[5,6] is smaller than the number with hypervariable sequence. For instance, hypervariability in CDR-H2 (the second CDR in the heavy chain) extends from residue V_H50 (heavy chain residue number 50) to V_H65, but a recent compilation of results from X-ray structures of antibody complexes does not show any in which residues between V_H59 and V_H65 are in contact with antigen.[1] The greater extent of hypervariability among the many sequences available presumably serves some purpose, and the generally smaller extent of antigen contact observed in X-ray structures is probably best attributed to a limited data base. We have recently found an antibody in which mutagenesis and binding data indicate that the extreme C-terminal end of CDR-H2 makes a large contribution to antigen binding.

Few antibody combining sites have been the subject of a thorough mutagenic probe to yield residue-specific binding data. Some studies have included mutations at residues that, according to X-ray structures of the relevant complex or a close homologue, are not in direct contact with antigen; therefore, the binding effects were attributed to indirect or long range effects.[7–10] Other studies have been performed without the benefit of X-ray structures of the antibody–antigen complexes in question, but have confirmed that specific framework residues can have a strong influence on antigen binding, presumably

Received July 1, 1993; revision accepted September 17, 1993.

Address reprint requests to Dr. Charles Eigenbrot, Department of Protein Engineering, Genentech, Inc., 460 Point San Bruno Blvd., South San Francisco, CA 94080-4990.

because they are intimately involved in presentation of CDR residues or contact antigen themselves.[11–15]

Murine antibody H52 (muH52) was raised[16] against the human β2-subunit (CD18) of the family of receptor proteins called integrins. CD18 is the common β-subunit of the three leukocyte integrins LFA-1, Mac-1, and p150,95 (see Hynes[17] for a review). These three integrins are restricted to cells of the immune system where they mediate cell adhesion events. They are required for leukocyte sticking at sites of inflammation. Monoclonal antibodies specific for CD18 have the potential to ameliorate a wide range of deleterious immunological and inflammatory processes.[18] We have sought to minimize potential immune system complications during the use of H52 in humans by performing antibody humanization.[19]

Transplantation of an antigen-binding surface from a nonhuman (e.g., mouse) antibody onto a human antibody framework, a process known as humanization, has become a popular way to circumvent some of the complications associated with the use of foreign antibodies in humans.[14,19–21] Various approaches to the selection of a human variable region framework have been pursued.[22] Our humanized antibodies are based on a common framework derived from a consensus sequence of the most common human antibody isotypes (V_HIII and $V_L\kappa$I) and include as few murine residues as possible in an attempt to minimize immunogenicity.[13] This results in murine residues being used only in CDRs and a few key framework residues.

The humanization of muH52 was less straightforward than that previously reported for the anti-$p185^{HER2}$ antibody 4D5.[13] In the 4D5 system, the initial version had a measurable affinity for its antigen, and the subsequent optimization involved testing a limited number of framework residues. The initial version transplanted almost exclusively CDR residues from the murine sequence, the definition of CDR used for this purpose being the restricted structurally derived one,[6] rather than the hypervariability definition.[4] A similar approach in the H52 system was unsuccessful. The initial nonbinding version was subjected to many framework substitutions in an attempt to find residues required for measurable binding. Far into this effort, the possibility that adding murine sequence in the C-terminal part of CDR-H2 (V_H59–V_H65) could make the key difference was tested. The resulting version was the first to have measurable binding in a cytometric assay. From this point, assay results were followed to determine which framework substitutions improved binding in the context of the additional murine CDR sequence. We chose to determine the structures of the two versions at opposite ends of the affinity spectrum to provide the clearest structural indication of the origin of the binding disparity possible. When we failed in our attempts to crystallize the Fab of the nonbinding initial version, the Fv of this version was produced and crystallized instead. A complete account of the humanization of muH52 will appear elsewhere (M. Zoller, manuscript in preparation).

The requirement of murine sequence from V_H59 to V_H65 raised two possibilities; either the additional murine sequence caused a significant remodeling of the archetypal antigen-binding surface atop the variable region, or a relatively small part of the antibody surface was responsible for a large fraction of the binding. In either case, the effect originates in a part of CDR-H2 not usually considered part of the direct antigen-binding function. To help discriminate between indirect and direct influences on binding, we have determined X-ray structures of fragments from both binding and nonbinding versions of the humanized H52 (huH52) antibody.

MATERIALS AND METHODS

Nomenclature

While creating various versions of huH52, both heavy and light chain genes were denoted alphabetically starting with "A," and then combined to form the name of the intact antibody. For instance, version "**AA**" combined heavy chain version "A," and light chain version "A," while version "**OZ**" combined heavy chain version "O" and light chain version "Z." Some letters were skipped. Kabat[4] residue numbering is used throughout.

Protein Production and Purification

A complete description of the humanization of H52 will be presented elsewhere (M. Zoller, manuscript in preparation). The genes encoding murine monoclonal antibody H52 (muH52) V_H and V_L domains were isolated by PCR amplification of mRNA derived from the corresponding hybridoma[16] (P. Berman, personal communication). Genes encoding humanized monoclonal antibody H52 version "**AA**" (huH52-**AA**) V_H and V_L domains were created by site-directed mutagenesis of previously described homologous genes.[14] Additional variants were created by site-directed mutagenesis[23] of huH52-**AA** variable domain genes (M. Zoller, personal communication). Chimeric H52 (chH52) was created by replacing human variable domain genes with the corresponding murine ones by subcloning and site-directed mutagenesis. Antibody fragments were secreted from *E. coli* hosts grown as previously described.[24] Fab fragments were released from corresponding fermentation pastes by partially digesting the bacterial cell wall with lysozyme followed by affinity purification on Streptococcal protein G as described for Fab′ fragments.[24] The huH52-**AA** Fv fragment was purified by thawing 100 g cell paste (from a total of 1340 g) in the presence of 100 ml of 0.1 M acetic acid (pH 2.8), 25 mM

EDTA, 1 mM PMSF over 30 min with gentle stirring. Cell debris was removed by centrifugation (30,000*g*, 10 min, 4°C). The resultant supernatant was passed over 100 ml DEAE fast flow sepharose (Pharmacia LKB) and loaded on to a 50 ml *Staphylococcal aureus* protein A controlled pore glass column (ProSepA, Bioprocessing limited). The column was washed extensively with 10 mM MES plus 10 mM EDTA at pH 5.5. The protein was then eluted with 3 M $MgCl_2$ at pH 6.5. The eluted protein was dialyzed into 10 mM MES at pH 5.5 and loaded on to a Mono S cation exchange column (Pharmacia LKB) and eluted with a gradient of 0 to 250 mM NaCl in 10 mM MES at pH 5.5. Chromatographic fractions were analyzed by SDS-PAGE and those containing similar amounts of V_L and V_H were pooled for crystallization.

Flow Cytometric Analysis of Fab Binding to Jurkat Cells

The Jurkat human acute T-cell leukemia cell line was purchased from the ATCC (Rockville, MD) and grown as recommended. Aliquots of 10^6 Jurkat cells were incubated with appropriate concentrations of selected Fab molecules in PBS plus 0.1% (w/v) BSA and 10 mM sodium azide for 45 min at 4°C. Cells were washed and then incubated with fluorescein-conjugated goat anti-human $F(ab')_2$ (Organon, West Chester, PA) for 45 min at 4°C. Cells were washed and analyzed on a FACScan® (Becton Dickinson, Mountain View, CA). Cells (8×10^3) were acquired by list mode and gated by forward light scatter vs. side light scatter excluding dead cells and debris.

Determination of Fab K_d by Competition Binding

HuH52 Fab fragments were iodinated with $Na^{125}I$ with Iodogen®. Briefly, 50 μg of Fab in PBS was placed in an Eppendorf tube coated with 50 μg of Iodogen® (Pierce). Carrier-free $Na^{125}I$ (Dupont/NEN) (1 mCi) was added. After 15 min, free ^{125}I was resolved from the labeled protein by chromatography on a PD-10® column (Pharmacia) preequilibrated with 0.5% gelatin in PBS. Antibody concentrations following iodination were determined by immunoassay.

Neutrophils were prepared using Lymphocyte Separation Medium® (Organon Teknika). After red blood cells were sedimented with 3% Dextran in 0.9% saline, leukocytes were layered on lymphocyte separation medium and centrifuged for 40 min at 400*g*. The supernatant was discarded and the residual red blood cells in the neutrophil pellet were cleared by hypotonic lysis with water, followed by an equal volume of 2× Hanks' balanced salt solution (HBSS). Neutrophils were centrifuged at 300*g* for 10 min and resuspended in HBSS containing 10 mM HEPES, 2% glucose, and 0.5% gelatin (HBSS+) at 5×10^6 cells/ml.

For competition binding determination of K_d, unlabeled Fab was titrated by 2-fold dilution in duplicate in situ in HBSS+ from 400 to 0 nM (huH52-**IA**), 200 to 0 nM (huH52-**OZ**), and 5 μM to 0 nM (huH42-**AA**). The corresponding ^{125}I-labeled Fab was added to give concentrations of 1, 0.5, and 65 nM, respectively. Neutrophils (850,000/well) were then added to the assays for huH52-**IA** and huH52-**OZ**; fewer neutrophils (500,000/well) were added to huH52-**AA** in order to achieve higher concentrations of Fab. Direct saturation binding was also attempted with huH52-**AA** to see if any specific binding could be detected. ^{125}I-labeled huH52-**AA** was titrated in situ in quadruplicate from 130 to 0 nM. HuH52-**AA** was added to 2 of the 4 resulting titrations series to give a concentration of 1.25 μM, and a corresponding amount of HBSS+ was added to the remaining series. All assays were incubated at room temperature for 2 hr with continuous shaking. The neutrophils were then harvested with a Skatron Combi Cell Harvester #11025® onto a 1.0-μm filtermat previously blocked with HBSS+. Filters were counted in an LKB Gammamaster 1277® counter. The data were analyzed by LIGAND,[25] according to the method of Scatchard.[26]

Crystallization and Data Collection

Crystals of huH52-**OZ** Fab grew in hanging drops made from reservoir and protein in a 1:3 ratio. The protein concentration was 10 mg/ml. The reservoir was 0.2 M calcium acetate, 0.1 M sodium cacodylate pH 6.5, and 9% (w/v) polyethylene glycol (PEG) 8000. A hexagonal plate approximately 0.35 × 0.35 × 0.10 mm was used for data collection in space group *P*3 with cell parameters $a = 101.$ and $c = 45.5$ Å. No crystals of the Fab of huH42-**AA** were obtained. Crystals of huH52-**AA** Fv also grew in hanging drops made from reservoir and protein in a 1:3 ratio, and a protein concentration of 10 mg/ml. The reservoir was 0.2 M ammonium acetate, 0.1 M sodium acetate pH 4.6, and 15% (w/v) PEG 3400. A plate-like crystal approximately 0.40 × 0.25 × 0.10 mm was used for data collection in space group *C*2 with cell parameters $a = 64.2$, $b = 61.3$, $c = 51.8$ Å, and $\beta = 99°$. Data were collected on an Enraf-Nonius FAST area detector using graphite monochromated CuK_α radiation from a Rigaku RU-200 rotating anode generator operating at 95 mA and 55 kV. Data collection and processing software included MADNES[27] and PROCOR.[28] Data collection and reduction statistics appear in Table I.

Structure Determination

huH52-OZ Fab

The structure was determined by molecular replacement (X-PLOR[29]) using the refined structure of hu4D5-4[30] as the basis for the search model. The actual search model lacked the CDR loops and the C-termini. To provide an aid in confirming any po-

TABLE I. Data Collection, Reduction, and Refinement Statistics for huH52 Fragments*

Resolution (Å)	Obs†	Unique‡	Mult§	% data**	R_{symm}††	R_{crys}‡‡
huH52-**AA** Fv						
15.0–4.06	2887 (2927)	1530 (1560)	501 (504)	.98 (1.00)	.0456	.193 (.196)
4.06–3.22	3044 (3136)	1544 (1589)	639 (658)	.98 (1.00)	.0492	.146 (.150)
3.22–2.82	2980 (3172)	1505 (1592)	657 (710)	.96 (1.00)	.0605	.174 (.183)
2.82–2.56	2805 (3082)	1447 (1563)	651 (731)	.92 (1.00)	.0761	.182 (.196)
2.56–2.38	2593 (2989)	1407 (1578)	613 (729)	.90 (1.00)	.0993	.206 (.225)
2.38–2.24	2449 (2855)	1353 (1537)	581 (707)	.86 (.98)	.1084	.201 (.210)
2.24–2.12	2290 (2683)	1313 (1464)	527 (672)	.84 (.94)	.1342	.209 (.219)
2.12–2.03	2181 (2622)	1250 (1429)	499 (661)	.80 (.92)	.1622	.208 (.220)
2.03–1.95	2055 (2472)	1226 (1382)	462 (621)	.78 (.88)	.1783	.217 (.230)
1.95–1.89	1639 (1954)	1001 (1118)	380 (500)	.64 (.70)	.2243	.231 (.240)
huH52-**OZ** Fab						
15.0–6.44	2205 (2241)	946 (950)	165 (169)	.90 (.91)	.0755	.270 (.297)
6.44–5.11	2387 (2469)	1006 (1013)	220 (221)	.95 (.96)	.0916	.177 (.197)
5.11–4.47	2111 (2150)	982 (986)	195 (201)	.94 (.94)	.0916	.141 (.158)
4.47–4.06	1890 (1949)	1001 (1013)	201 (206)	.95 (.96)	.1163	.154 (.184)
4.06–3.77	1701 (1780)	970 (993)	185 (193)	.95 (.97)	.1370	.165 (.175)
3.77–3.54	1670 (1787)	1012 (1058)	170 (186)	.93 (.97)	.1611	.181 (.196)
3.54–3.37	1570 (1700)	950 (1004)	170 (185)	.92 (.98)	.1800	.176 (.199)
3.37–3.22	1558 (1742)	979 (1046)	180 (212)	.92 (.98)	.2153	.201 (.223)
3.22–3.10	1371 (1602)	929 (1031)	137 (171)	.89 (.99)	.2559	.210 (.250)
3.10–2.99	1279 (1593)	885 (1011)	129 (198)	.85 (.97)	.2952	.235 (.264)

*Values in first 4 columns are for all data except when an additional value appears in parenthesis, in which case the number outside parenthesis is for data with $F/\sigma \geq 2$ only.
†Number of measurements.
‡Number of unique reflections.
§Number of unique reflections for which multiple measurements were made.
**Fraction of total possible unique reflections actually measured.
††$R_{symm} = (\Sigma|I-<I>|)/\Sigma I$ and includes all reflections with $I>0$.
‡‡$R_{crys} = (\Sigma||F_o| - |F_c||)/\Sigma|F_o|$ for data with $F/\sigma \geq 2$. The values for all data with $I>0$ are given in parentheses.

tential molecular replacement solution, all cysteines and tryptophans were truncated to alanine. The cross-rotation search and subsequent Pc refinement[31] both gave a single unambiguous signal. The correct translation was determined in a correlation coefficient search in the *ab* plane using squared normalized structure factors, and yielded a correlation coefficient of 0.47 (16 σ above the mean). The *R*-value for the top result was 39.9% for data 8.0–3.5 Å resolution.

huH52-AA *Fv*

The search model for this structure determination was the variable region of the partially refined huH52-**OZ** Fab fragment. The CDR loops and chain termini were not included. The cross-rotation search and Pc refinement gave an unambiguous result. The oriented model gave a correlation coefficient between calculated and observed squared normalized structure factors of 0.49 (5 σ above the mean) in a translation search of the *ac* plane. This complete solution gave an *R*-value of 51.2% for data 10–3 Å.

Structure Refinement

huH52-OZ *Fab*

A great majority of the residues excluded from the search model were clearly seen in $2F_o-F_c$ maps calculated after rigid-body refinement at 3 Å (Fig. 1). Several cycles of model building and positional refinement yielded a model with an *R*-value of 19.8%. Simulated annealing (SA) refinement at 3 Å reduced the *R*-value to 17.8%. Refinement of individual *B*-factors employed very tight restraints (Table II). No solvent is included in the final model.

huH52-AA *Fv*

A random 10% of the data was sequestered from refinement for calculation of "free" *R*-values.[32] Rigid-body refinement against data 15–4 Å and then 10–3 Å gave *R*-values (nonsequestered and sequestered data, respectively) of 47.6 and 49.9%. Inspection of a 3 Å $2F_o-F_c$ map allowed addition of 495 atoms (from all or part of 63 residues), representing a large majority of the sequence absent from the original search model. Refinement and adjustments to the model were made as the resolution was increased from 3.0 to 2.5 Å, and finally to 1.9 Å. The entire model was inspected using a series of σ_A-weighted SA-omit maps[33,34] during refinement at both the 3.0 and 1.9 Å resolution stages. No complete trace for CDR-H3 could be identified. Because of ambiguity in the main chain trace, some relatively well-ordered residues in this CDR were removed from the final model, and these persist

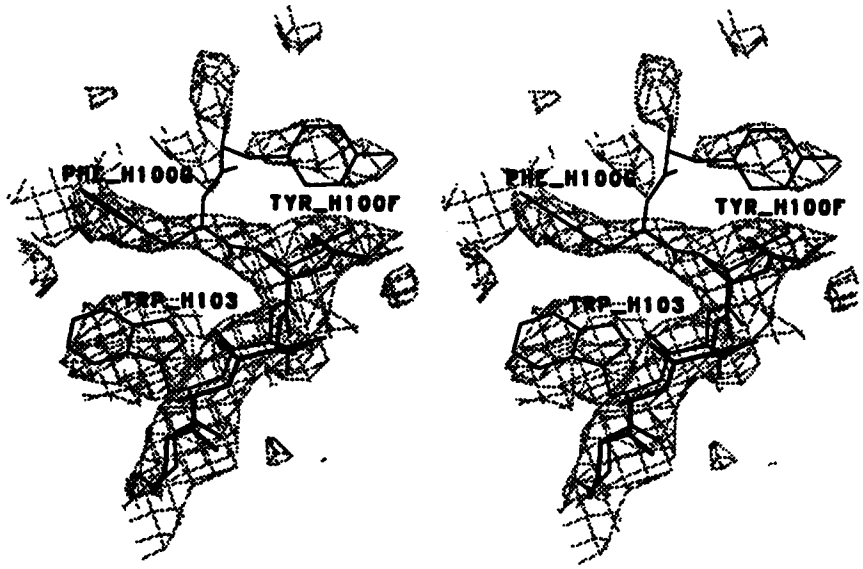

Fig. 1. $2F_o-F_c$ electron density map confirming the huH52-**OZ** Fab molecular replacement solution. The phasing model was the rigid-body refined search model (heavy lines). Depicted is a region at the C-terminal end of CDR-H3 in which some residues excluded from the search model are clearly indicated (thin lines). The middle part of CDR-H3 could not be traced, is absent from the final model, and presumably adopts multiple configurations in the crystal.

TABLE II. Refinement Statistics for huH52 Antibody Fragments

	huH52-**AA** Fv		huH52-**OZ** Fab	
Refinement resolution (Å)	10.0–1.9		10.0–3.0	
Number reflections ($F/\sigma F \geq 2$)	13122		9146	
Completeness overall ($F/\sigma F \geq 2$)	94%		90.5%	
Completeness at limit ($F/\sigma F \geq 2$)	80%		76.1%	
R-value ($F/\sigma F \geq 2$)	0.180		0.178	
R-value no solvent ($F/\sigma F \geq 2$)	0.228		0.178	
rmsd bond distances (Å)	0.013		0.019	
rmsd bond angles (°)	2.8		3.8	
rmsd ω (°)	5.0		6.5	
rmsd dihedrals (all) (°)	26.6		27.3	
rmsd improper dihedrals (°)	1.6		1.5	
Number of atoms	1852		3260	
Number of atoms occ. = 0	14		43	
Number of residues	227		434	
Number of waters	109		0	
Average B-factor for occ. = 1 (Å^2)	15.5		15.9	
Average solvent B-factor	29.1		—	
	Target	Found	Target	Found
rmsd main chain B-factors (bond)	1.0	1.8	0.15	1.2
(angle)	1.5	2.9	0.15	2.1
rmsd side chain B-factors (bond)	1.5	3.3	0.15	1.2
(angle)	2.0	4.8	0.15	1.9

among the largest positive features in the final difference maps. The final R-values for unsequestered and sequestered data are 18.0 and 23.9%, respectively. Representative electron density for the final huH52-**AA** Fv model appears in Figure 2, and a metrical summary of the final models appears in Table III. Plots of temperature factors appear in Figure 3. Coordinates of the final models will be deposited in the Protein Data Bank at Brookhaven National Laboratory, Upton, NY.

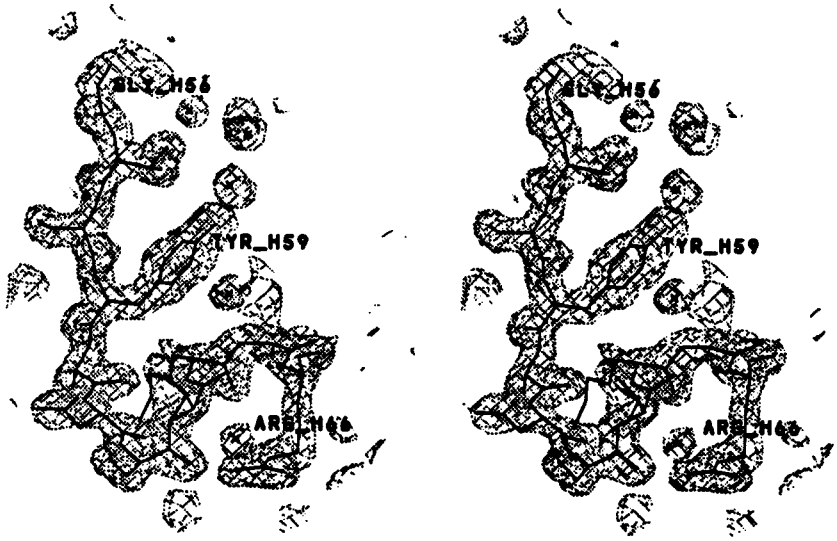

Fig. 2. $2F_o-F_c$ electron density map phased by the final huH52-**AA** Fv model at 1.9 Å resolution. The region depicted is the C-terminal end of CDR-H2 where the sequence of residues V_H59 to V_H65 differs between the binding and nonbinding versions.

TABLE III. Domain Relationships* for huH52 Antibody Fragments

	huH52-**OZ** Fab	huH52-**AA** Fv
V_L–V_H		
rmsd(Å)	1.10	0.95
Shift(Å)	0.26	0.16
Angle(°)	170	176
C_L–C_{H1}		
rmsd(Å)	1.13	
Shift(Å)	1.59	
Angle(°)	168	
Elbow(°)	135	

*The table values result from least-squares superpositioning of selected Cα atoms from a pair of domains. Rotation of one domain around the pseudo 2-fold axis by the indicated angle, followed by the indicated shift, yields the indicated rms deviation among the selected Cα atoms. For the V_L–V_H calculation the following Cα atoms were used: V_L, 11–26, 32–39, 45–48, 61–67, 70–91, and 97–105. V_H, 10–25, 33–40, 46–49, 66–72, 77–95, and 102–110. For the C_L–C_{H1} calculation the following residues were used: C_L, 111–120, 130–149, 159–162, 172–181, 193–198, and 205–208. C_{H1}, 117–126, 136–155, 163–166, 175–184, 195–200, and 207–210.

RESULTS

Binding of Fab Fragments to Jurkat Cells

Binding of Fab fragments from different huH52 variants was investigated by flow cytometry (Fig. 4). The huH52-**IA** Fab shows an EC_{50} only about 60-fold worse ($EC_{50} \approx 0.25$ vs. 0.0042 nM) than that of the chimeric H52. HuH52-**AA** Fab shows no detectable binding at the highest concentration used, and behaves across the tested range like the negative control Fab specific for another antigen. The only sequence changes between huH52-**AA** and huH52-**IA** are those 7 from V_H59 to V_H65 (Fig. 5). HuH52-**OZ** behaves most like the chimeric Fab ($EC_{50} \approx 0.040$ nM). There are 5 sequence differences between huH52-**IA** and huH52-**OZ** (Fig. 5) which together cause a marginal improvement in binding.

Fab Binding Affinities

The competition binding assay yielded K_d values for the Fab fragments of huH52-**IA** and huH52-**OZ** of 51 and 4 nM, respectively. No specific binding of huH52-**AA** was observed under any circumstances. This suggests that the K_d for this version is, conservatively, >6 μM, the largest dissociation constant we have observed utilizing these methods.

Description of the Structures

The quaternary structures are similar to those previously found for antibody fragments[35–37] and appear in Table III. The elbow angle found for huH52-**OZ** fAB (135°) is at the low end of the range previously reported.[38] The (ϕ,ψ) main chain torsion angles plotted in a Ramachandran diagram indicate there is one high energy combination in huH52-**AA** Fv. Thr V_L51 has (ϕ,ψ) = (64,−50) and is found in CDR-L2. This conformation is characteristic of the many structures with this class of CDR-L2.[39] The huH42-**OZ** Fab has this and 5 additional questionable (ϕ,ψ) angles. Residue V_L69 has (ϕ,ψ) = (67,141) in huH52-**OZ** Fab. This differs by a peptide flip from the (ϕ,ψ) = (−101,−14) seen in huH52-**AA** Fv. There is no indication in the huH52-**OZ** Fab 3 Å electron density maps that such an adjustment would be a better fit, but the

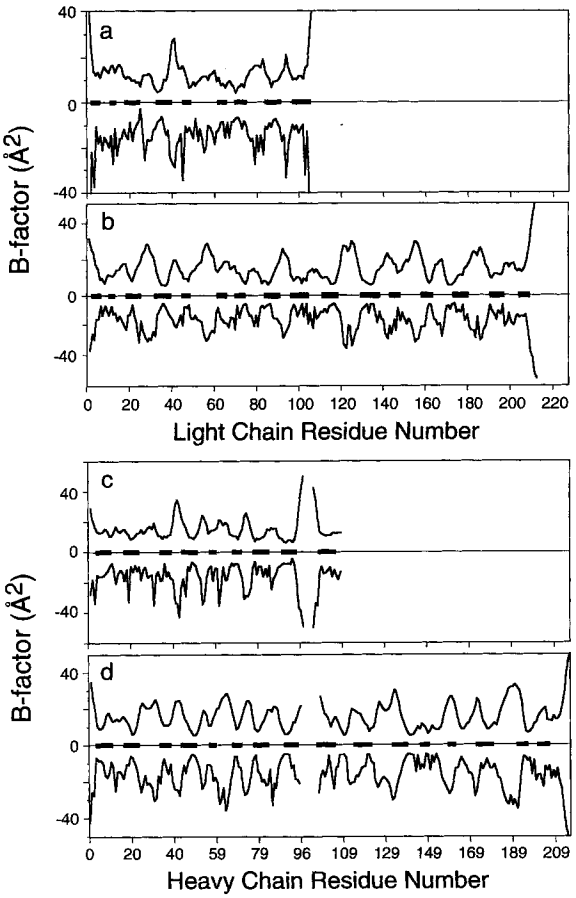

Fig. 3. Average *B*-factors by residue for main chain atoms (upward increasing) and side chain atoms (downward increasing). (**a**) huH52-**AA** Fv light chain, (**b**) huH52-**OZ** Fab light chain, (**c**) huH52-**AA** Fv heavy chain, and (**d**) huH52-**OZ** Fab heavy chain. The thick sections along $B=0$ denote β-strands. The discontinuities occur where residues could not be placed due to poor electron density (disorder). Where *B*-factor values exceed the range of the plot (at chain termini), the maximum values are (**a**) N-terminus $B=40$ (main chain) and 51 Å^2 (side chain); (**b**) C-terminus, $B=54$ (main chain) and 55 Å^2 (side chain); (**d**) C-terminus, $B=55$ (main chain) and 56 Å^2 (side chain).

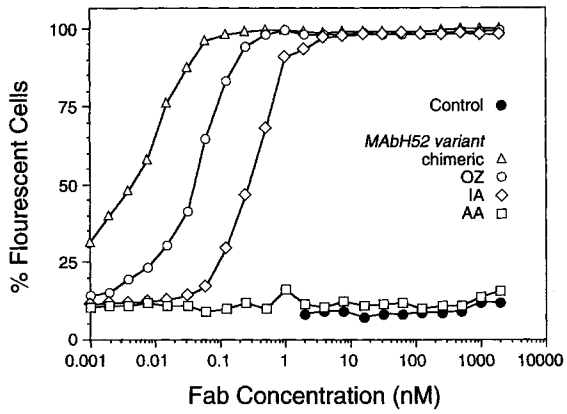

Fig. 4. Flow cytometric analysis for binding of Fab fragments to Jurkat cells. The control Fab is hu4D5-8.[13]

huH52-**AA** Fv trace is nonetheless almost certainly applicable to huH52-**OZ** Fab too. The others are in poorly ordered regions near chain termini at V_H95 (CDR-H3 is disordered beyond this residue), V_H204, V_H213, and V_H214. There are *cis*-peptide bonds at prolines V_L8 and V_L95 for both molecules, and for the constant domains of huH52-**OZ** at prolines V_L141, V_H447, and V_H449. The estimated error in the atomic coordinates determined by the method of Luzatti[40] is ≈0.22 Å for huH52-**AA** Fv.

Symmetry-related molecules are partners in direct H-bonding interactions for both molecules. In the huH52-**AA** Fv structure, there are three β-sheet H-bonds 2.9 Å long centered on a crystallographic 2-fold axis adjacent to residues V_L9, V_L10, and V_L12. Another less extensive interaction is found at V_L69 also involving protein atoms directly [Thr V_L69 Oγ1 to Leu V_H11 N (3.0 Å) and Thr V_L69 N to Gly V_H9 O (3.1 Å)]. Water mediated H-bonds are apparent in the regions between V_H56 and V_H28 and between 2-fold related V_H53 regions. The 3.0 Å huH52-**OZ** Fab structure includes no explicit water molecules, but there are regions where symmetry-related molecules are close enough to suggest well-ordered waters would be apparent at higher resolution. These include the regions between V_L26 and V_H133 and between V_H55 and V_H155/V_H192. There are 3 main chain to side chain H-bonds from 2.6 to 3.3 Å long between residues $V_L64/66/67$ and $V_L151/152$. There is one main chain to main chain H-bond 2.9 Å long from V_L9 to V_L201.

The sequence of 5 of the 6 CDRs is sufficient to predict their main chain conformation with reasonable accuracy.[6] The final CDR, CDR-H3, has a section so poorly ordered in both huH52 structures as to be indeterminable. In the parent muH52 and these humanized versions, CDR-H3 is 12 amino acids long. In the huH52-**AA** Fv structure, we were able to confidently determine the positions of residues up to Leu V_H98 and from Asp V_H100C. In huH52-**OZ** Fab we determined up to V_H96 and from V_H100E but truncated the side chains for V_H95, V_H96, and V_H100E (Trp, Arg, and Arg) to Cβ.

Comparison Between Structures

The principal result from the comparison of huH52-**AA** Fv and huH52-**OZ** Fab concerns changes in the C-terminal portion of CDR-H2 where the murine sequence was applied for an additional 7 residues in huH52-**OZ** (Figs. 5, 6). Figure 7 shows that the largest concerted, directional structural shift between these structures occurs in this region. This was determined by first superpositioning the main chain atoms (N, Cα, C, O) of the two structures (omitting some terminal residues and the absent CDR-H3), then summing all vectors between corresponding main chain atoms in a moving 7 residue

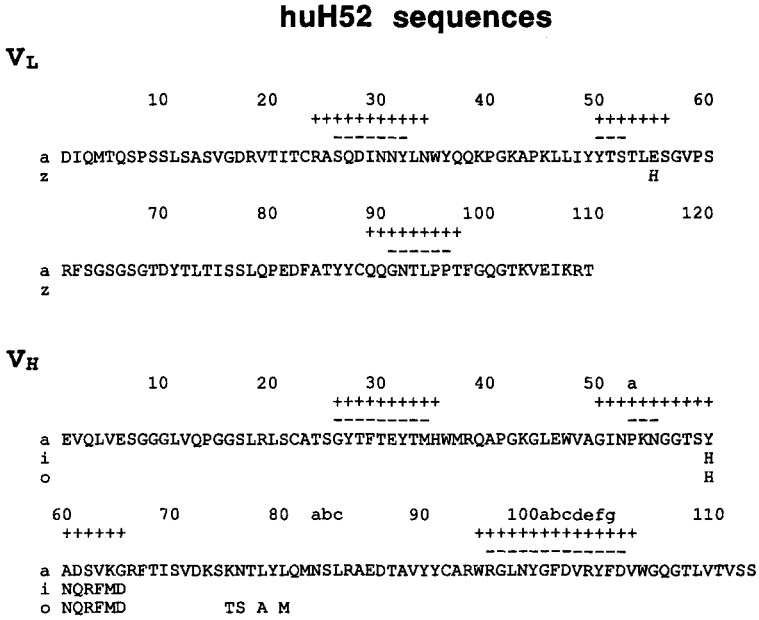

Fig. 5. Amino acid sequence of huH52 variable domains. The initial versions for both V_L and V_H are called "a," and changes are indicated only for the subsequent versions indicated by a one letter code. Hypervariable regions[4] are indicated by "+" and structurally defined CDR regions[6] by "–."

window.[41] This technique identifies relatively small regions that share a net directional shift from one molecule to another. Our choice of a 7 residue window reflects a balance between sensing large but local shifts and sensing shifts in the loops common to immunoglobulin domains.

Included in Figure 7 is an indication of intermolecular contacts in the two different crystal lattices. The presence of different intermolecular environments for the crystal structures under study complicates the analysis of their differences. We have shown that when a region experiences an intermolecular contact in any or all of the structures being compared, it prevents a straightforward attribution of structural change to other influences.[42,43] It is possible that such contacts are partially responsible for the maximum at residue V_H53, in the N-terminal half of CDR-H2, where both huH52-**AA** and huH52-**OZ** have intermolecular contacts. However, most of the larger maximum at V_H61 can be attributed to a sequence change at V_H65- from Gly in huH52-**AA** to Asp in huH52-**OZ.** The glycine adopts a main chain configuration ($\phi,\psi = 93°,-31°$) not ordinarily accessible to other amino acids. Indeed, the huH52-**OZ** Asp has ($\phi,\psi = -67°,-52°$), and residues V_H61–V_H66 are all in the helical region. In huH52-**AA,** this helical segment is interrupted by Lys V_H64 ($\phi,\psi = -56°,130°$) as well as Gly V_H65. The result is a shift of about 2.7 Å for the Cα atom of residue V_H65. Main chain torsion angles in CDR-H2 are otherwise quite similar, and the structural change is accommodated in a relatively small section of adjoining polypeptide. The Cα shift is down to 0.4 Å by residue V_H69.

The section immediately toward the N-terminus from V_H65 shows an H-bond [Asn V_H60 Nδ2–Trp V_H47 O (2.9 Å)] and a salt bridge [Arg V_H62 Nη1–Glu V_H46 Oϵ2 (2.9 Å)] that are present in huH52-**OZ** but absent in huH52-**AA.** The huH52-**AA** sequence (Ala V_H60, Ser V_H62) does not provide the opportunity for these interactions. There are also intermolecular contacts in both molecules. Together, these influences contribute to the somewhat longer interval before Cα shifts are reduced (to 1.0 Å) at V_H59.

The main chain of the archetypal antigen-binding surface does not differ significantly between the two versions. This can be seen in Figure 7, in which the CDRs do not correlate with prominent maxima. For CDR-H1, differences in the intermolecular environments are likely to have caused a larger difference than would otherwise have been seen. In addition, the rms deviations in Table IV reveal that the CDRs taken together as a group match quite well (rms deviation of Cα atoms 0.67 Å).

There are two other segments where the sequences of huH52-**AA** and huH52-**OZ** differ. Residue V_L55 is Glu in huH52-**AA** and His in huH52-**OZ.** Figure 7a indicates only moderate concerted main chain shifts around this site. The structural shifts observed are probably at least partly due to the intermolecular contacts both structures experience in this region. There are also sequence differences at V_H75, V_H76, V_H78, and V_H80. The Leu→

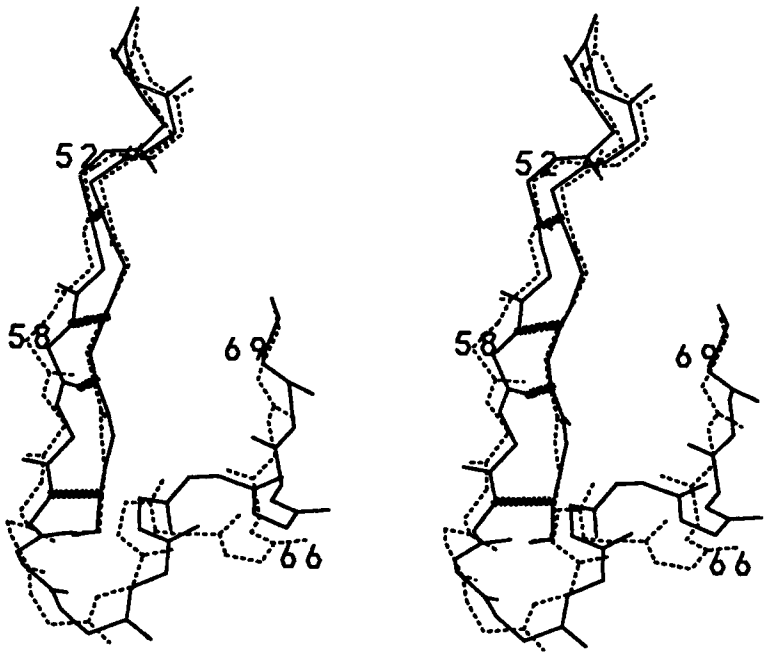

Fig. 6. Stereo view of main chain atoms from huH52-**AA** (solid) and huH52-**OZ** (dotted) in the segment V_H48–V_H69, superposed using residues V_H48–V_H52. Main chain dihedral angles differ for V_H64 and V_H65, creating a peptide flip for the link between them and large shifts for V_H65. Note the β-sheet H-bonds (wide gray lines) separating the N-terminal part of CDR-H2 from the C-terminal part.

Met change at V_H80 is conservative, and although the Leu→Ala change at V_H78 is less so, both residues are in the β-sheet with their side chains directed away from solvent (and away from direct interaction with antigen). The side chains of residues V_H75 and V_H76 are more exposed and are found adjacent to CDR-H1 and the rest of the archetypal binding region. Figure 7b shows there are only minor structural shifts in the region V_H75 to V_H80.

DISCUSSION

Our interest in determining these two crystal structures was in finding structural indications of their very different binding affinities—one has a K_d of 4 nM, the other is conservatively estimated as >6 μM. The two versions have different amino acids at a total of 12 sites, concentrated in three distinct regions. For reasons we discuss below, we believe most of the binding affinity effect derives from sequence differences in the C-terminal part of CDR-H2, V_H59–V_H65. Speculation regarding the structural influences on their binding affinities requires we assume that Fab fragments bound and unbound to CD18 are structurally similar. There are examples where X-ray structures of Fab with and without antigen differ considerably,[44,45] but such cases are so far restricted to cases involving small antigens, for example, peptides and pieces of single-stranded DNA. The only two examples in which an antibody fragment has been studied both with and without protein antigen involve the antibody D1.3. The structure of D1.3 Fv with and without antigen (lysozyme), despite a small rearrangement between V_L and V_H, adopts no significant changes in the CDR residues,[46,47] while changes are restricted to side chains when the D1.3 Fab binds an antiidiotypic Fab.[47] In addition, the effects of site-directed mutagenesis on antibody–antigen affinities are generally interpretable on the basis of a relatively invariant antibody structure.[30,48]

In both of the two huH52 X-ray structures reported here there is no clear electron density for several residues in the middle of CDR-H3, so we are unable to determine how they differ in this region. We observed a similarly variable CDR-H3 in the hu4D5 X-ray structures, and in that case attributed the large differences to different intermolecular environments within the crystal.[30] Kossiakoff et al. have shown, however, that intermolecular crystal forces only select from the conformations present in solution as part of a protein's normal dynamism, rather than inducing new conformations.[42] This being the case, the disordered CDR-H3 in the huH52 structures is most likely a reflection of a highly mobile solution structure. Since the distance between CDR-H3 and the last part of CDR-H2 is large (> 13 Å), it is unlikely that sequence changes V_H59 to V_H65 alter CDR-H3 in an important way. Based on this reasoning and the D1.3 precedent, we assume

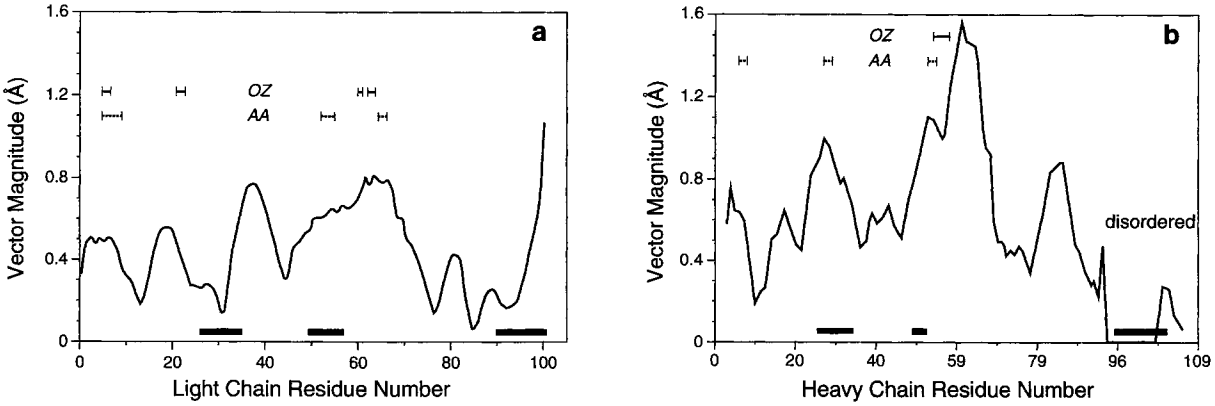

Fig. 7. Vector shift magnitudes after superpositioning of huH52-**AA** Fv and huH52-**OZ** Fab variable regions, calculated for main chain atoms only in a 7 residue moving window. CDR regions (structural definition[6]) are indicated across the bottom by dark bars. Regions of intermolecular contact are indicated for huH52-**AA** Fv (dotted) and huH52-**OZ** Fab (solid), respectively, above the curve. (**a**) V_L residues, (**b**) V_H residues. Part of CDR-H3 could not be located in either structure.

TABLE IV. Rms Deviations After Superpositioning of Cα Atoms*

	huH52-**OZ** Fab				hu4D5-8(I)				hu4D5-8(II)			
	All	fwk	cdr	cdr'	All	fwk	cdr	cdr'	All	fwk	cdr	cdr'
huH52-**AA** Fv	.89	.86	.67	1.03	.70	.54	1.02	1.03	.74	.56	1.03	1.04

*Cα atoms of residues V_L1–V_L107 and V_H1–V_H95, V_H100F–V_H105 ("all") were used to calculate the rms deviations. Residues V_H96–V_H100E, which comprise most of CDR-H3 and many of which were not found in electron density maps, were not included. The comparisons are broken into three subsets: "fwk" denotes just the framework Cα atoms included in "all," and "cdr" the combined CDR and V_L66–V_L68 loops (as a single unit) included in "all." (The V_L66–V_L68 loop is anomalous in the 4D5 structures due to an unusual sequence. Also, the hu4D5 structures appeared in a two molecule asymmetric unit.[30]) The "cdr'" subset extends the residues included in CDR-H2 to V_H65.

changes in huH52 on binding CD18 are small or similar to its normal dynamism.

The binding affinities of the huH52-**AA** and huH52-**OZ** Fabs are quite different (Fig. 4). The affinity of huH52-**AA** puts it below the detection limit of the FACScan assay, while huH52-**OZ** approaches the affinity of chH52. These results were confirmed by a subsequent competition binding assay, even to the extent that no specific binding of huH52-**AA** was detected under any conditions (see Methods and Materials). Most of the improvement in the antigen binding affinity of huH52-**OZ** can be traced to the murine sequence incorporated in the C-terminal end of CDR-H2. This region is, by a structurally derived definition, not part of the CDR.[6] On the other hand, the statistical sequence hypervariability characteristic of CDRs does extend into this region.[4] In addition, this segment is largely exposed to solvent and available for participation in the antigen–antibody interface. HuH52-**OZ** extends murine sequence vs huH52-**AA** by 7 additional residues, from V_H59 to V_H65 (Fig. 5). Since our results show the structures differ most in this region (Fig. 7) and almost not at all in the archetypal binding surface (Fig. 7, Table IV), we conclude that the binding effect derives from interactions between the last part of CDR-H2 and antigen. This suggests that a large part of the huH52-**OZ** binding affinity resides in the side chains of this latter part of CDR-H2 and/or the relatively large but local differences around V_H65. X-Ray structures of antibody fragments complexed with protein antigens have shown that the N-terminal part of CDR-H2 is intimately involved in creation of the binding interface.[2] However, the region V_H59–V_H65 of CDR-H2 has not been seen in contact with antigen.[1]

There is the intriguing possibility that the difference in the V_L/V_H relationship between huH52-**AA** and huH52-**OZ** is responsible for the binding affinity effects. Table V presents comparisons of the V_L/V_H relationships among the huH52 and hu4D5 structures. Although the 5.2° rotation angle relating the huH52-**AA** and huH52-**OZ** V_H domains after superposition of their V_L domains is near the low end of analogous values reported by Lascombe et al.,[49] the highly similar sequences among the huH52 and hu4D5 molecules suggests there may be something unique about the V_L/V_H relationship in huH52-**OZ**. Figure 8 illustrates the huH52-**AA** and huH52-**OZ** V_H domains after their V_L domains have been superposed by the method of Colman et al.[50] The difference in position of the CDR residues could be re-

TABLE V. Variable Domain Relationships*

	huH52-**AA**	huH52-**OZ**	hu4D5-8(I)	hu4D5-8(II)	hu4D5-4(I)	hu4D5-4(II)	hu4D5-7(I)	hu4D5-7(II)
huH52-**AA**		.26	.24	.28	.31	.32	.32	.38
		.31	.25	.25	.27	.27	.30	.32
huH52-**OZ**	5.2		.33	.32	.32	.30	.32	.34
	.03		.34	.32	.31	.36	.35	.35
hu4D5-8(I)	2.4	4.1		.15	.24	.27	.27	.34
	.14	.35		.18	.26	.28	.24	.29
hu4D5-8(II)	3.3	3.8	1.0		.24	.26	.24	.31
	.13	.29	.01		.27	.27	.25	.28
hu4D5-4(I)	4.2	5.7	2.2	1.9		.19	.21	.23
	.17	.31	.09	.05		.19	.18	.25
hu4D5-4(II)	3.1	5.8	1.9	2.1	1.4		.18	.21
	.23	.38	.10	.08	.09		.25	.24
hu4D5-7(I)	3.3	4.5	1.3	0.8	1.4	1.5		.21
	.08	.24	.08	.01	.05	.13		.26
hu4D5-7(II)	1.7	5.7	1.8	2.6	2.7	1.5	2.3	
	.27	.32	.05	.06	.04	.00	.04	

*Upper right triangle reports rms deviation of selected V_L (upper number) and V_H (lower number) Cα atoms after superpositioning. The selected atoms are from V_L residues 33–39, 43–47, 84–90, and 98–104 and V_H residues 34–40, 44–48, 88–94, and 103–109.[50] The lower triangle reports the rotation angle (in degrees, upper number) and shift (in Å, lower number) required to superpose the selected V_H atoms after they were transformed according to the superpositioning of the selected V_L atoms. All three hu4D5 molecules crystallized with two molecules in the asymmetric unit.

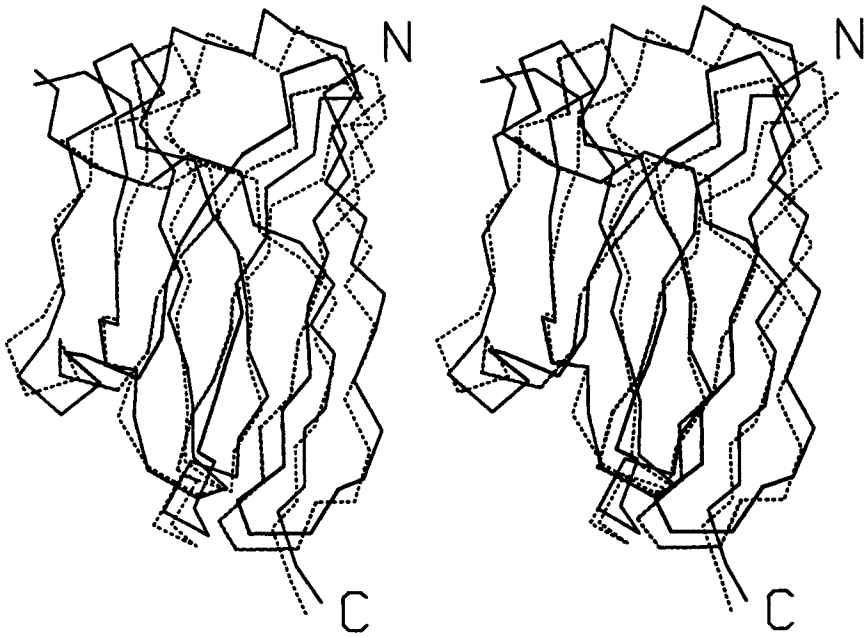

Fig. 8. Stereo image of Cα atoms of V_H domains of huH52-**AA** (solid lines) and huH52-**OZ** (dotted lines) after superpositioning of their respective V_L domains using selected Cα atoms.[50] The view is along the axis about which a 5.2° rotation will minimize the rms deviation. V_H domain termini are labeled. A break in CDR-H3 is apparent at the upper left, and CDR-H2 is on the left.

sponsible for the profound difference in binding affinities. However, care must be taken in reaching such a conclusion, since the mechanism by which sequence changes might cause this shift is difficult to discern. Tulip et al. have discussed a possible connection between the V_L/V_H relationship and the surface area buried within the interface,[37] but such differences in the huH52 system must be small, and in any case the calculation is complicated by the absence or variability of parts of CDR-H3. Other cave-

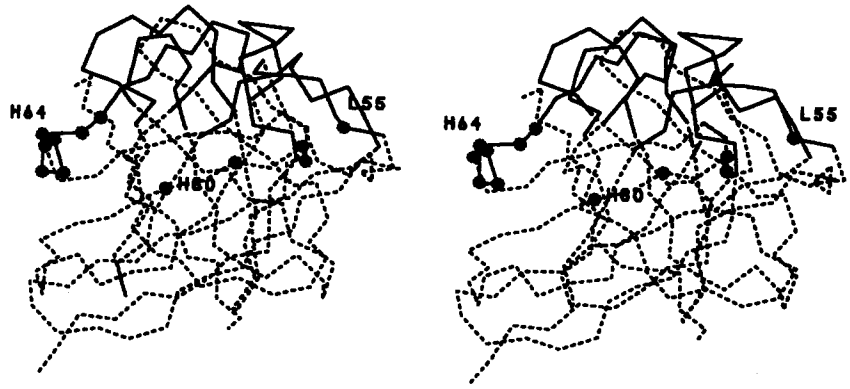

Fig. 9. Stereo image of Cα atoms of huH52 variable region indicating the residues where the sequences of huH52-**AA** and huH52-**OZ** differ. Framework residues are depicted with dotted lines, CDR residues with solid lines, and residues subject to sequence change with dotted spheres. There are three segments where differences occur—at V_L55, all the residues V_H59–V_H65, and residues V_H75, V_H76, V_H78, and V_H80.

ats for this interpretation include the possible influence of intermolecular packing forces[50] and the fact that huH52-**AA** is an Fv structure while huH52-**OZ** is an Fab. One observation that may be important is the 1.5 Å shift of the Trp V_H47 side chain that accommodates the large shift in the proximal part of CDR-H2. The other V_H interface residues are much less effected.

The possibility that the C-terminal part of CDR-H2 exerts its effect on binding by one or more other indirect mechanisms cannot be completely eliminated. However, if the region V_H59–V_H65 influences the N-terminal part of CDR-H2, it would have to do so despite the intervening β-sheet main chain H-bond interactions between V_H48–V_H52 and V_H56–V_H60. It is also unlikely to limit the conformations available to the N-terminal part of CDR-H2 in the way that loss of a salt bridge at the base of CDR-H3 might change CDR-H3's role in binding.[9] Any of the other interactions between V_H59–V_H65 and the rest of the molecule could, in principle, influence a part of the antibody that contacts antigen directly while remaining free of contact itself. The weight of the evidence, however, points to direct antigen contact for one or more of the residues from V_H59 to V_H65.

Without an X-ray structure of the huH52/CD18 complex, we are unable to distinguish whether the effect of murine sequence for V_H59–V_H65 occurs through side chains on a relatively invariant main chain, or if the large but local changes (including main chain) caused by changing V_H65 from Gly to Asp are the predominant contributors. It is possible that among the seven changed side chains, only one is important, and it could act across a large distance. Such a mechanism has been proposed by Chien et al.[8] to explain the loss of phosphocholine binding when an Asp 9 Å from the antigen binding site is changed to Ala. Inspection of other antibody structures in the PDB does not suggest any particular correlation between the presence of Gly or non-Gly amino acids at V_H65 and antigen binding. The question is amenable to investigation using only selected murine residues in the V_H59–V_H65 region. The importance of this segment for binding of two other humanized antibodies is known. Murine sequence aided the binding of a humanized anti-CD3 antibody,[51] but had the opposite effect for the humanized anti-$p185^{HER2}$ (hu4D5).[52] In another related system involving a different antigen specificity, there is mutagenic evidence that having murine residues at V_H60 and V_H61 is important but that the human consensus Gly serves as well as the murine Asn at V_H65.[53]

The foregoing attribution of large binding affinity effects to the C-terminal part of CDR-H2 relies on an additional assumption—that the two other regions of sequence difference between huH52-**AA** and huH52-**OZ** (which together comprise the sequence differences between huH52-**IA** and huH52-**OZ**, see Fig. 5) are structurally the same in huH52-**AA** and huH52-**IA**. This assumption requires that each of the three regions with different sequence reacts to mutation without affecting either of the other two. Residue V_L55 is certainly remote from the other two regions (Fig. 9) and its highly exposed side chain is unlikely to cause large or remote structural change. Though the regions V_H59–V_H65 and V_H75–V_H80 are nearer to each other, any transmission of structural change between them would necessarily occur via a β-sheet, and we and others have shown that β-sheets are the secondary structure element most resistant to change upon mutation.[43,54,55] The Leu→Met substitution at V_H80 is a conservative one, but even the Leu→Ala substitution at V_H78 is not expected to cause large shifts, based on an identical substitution among the hu4D5 X-ray structures.[30] The side chains of residues V_H75 and V_H76 are exposed to solvent and therefore are also not likely to cause structural change at remote sites.

Figure 7b confirms there are only minor main chain differences in the segment V_H75–V_H80.

CONCLUDING REMAKRS

The humanization of the anti-CD18 antibody H52 was hampered by not appreciating the possibility that residues in the C-terminal part of CDR-H2 could be important in antigen binding. We determined crystals structures of both a tight-binding and a nonbinding version of the humanized antibody, and found large (2.7 Å at V_H65 Cα) and local structural differences, concentrated in the region V_H59–V_H65. Based on precedents in the D1.3 antibody system, we assume these structures are close to those existing after binding to CD18. Because there are only minor differences found in the other CDR regions, we conclude that the changes in the C-terminal part of CDR-H2 are responsible for the large difference in binding affinity, and suggest the most straightforward mechanism for the effect is by direct contact between this region and CD18. This part of a CDR-H2 has not been observed in contact with antigen in the antibody–antigen complex X-ray structures reported so far.

The structures reported herein share highly homologous framework region sequences with the hu4D5 fragments for which we have previously reported X-ray structures.[30] There are only 6 framework sequence differences between huH52-**AA** and hu4D5-8. The structural similarity of these two families of humanized antibodies is seen in the 0.55 Å rms deviation between huH52-**AA** Fv and hu4D5-8 Fv (Table IV) and in the quaternary relationships in Tables III and V. This is demonstration of the relative independence of framework and CDR regions in this system. Our ability to mimic native binding affinities for this and other humanized antibodies[13,51] suggests the use of a common framework will provide sufficient flexibility for other antibody humanization efforts.

ACKNOWLEDGMENTS

We thank our colleagues at Genentech: Mike Covarrubias and Brad Snedecor for *E. coli* fermentations of Fab and Fv fragments; Mark Vasser, Parkash Jhurani, and Peter Ng for synthesizing oligonucleotides; and Bob Kelley for helpful discussions.

REFERENCES

1. Padlan, E.A., Kabat, E.A. Modeling of antibody combining sites. Methods Enzymol. 203:3–21, 1991.
2. Davies, D.R., Padlan, E.A., Sheriff, S. Antibody-antigen complexes. Annu. Rev. Biochem. 59:439–473, 1990.
3. Wilson, I.A., Stanfield, R.L. Antibody-antigen interactions. Curr. Opin. Struct. Biol. 3:113–118, 1993.
4. Kabat, E.A., Wu, T.T., Perry, H.M., Gottesman, K.S., Foeller, C. "Sequences of Proteins of Immunological Interest," 5th ed. Bethesda, MD: National Institutes of Health. 1991.
5. Tramontano, A., Chothia, C., Lesk, A.M. Framework residue 71 is a major determinant of the position and conformation of the second hypervariable region in the V_H domains of immunoglobulins. J. Mol. Biol. 215:175–182, 1990.
6. Chothia, C., Lesk, A.M. Canonical structures for the hypervariable regions of immunoglobulins. J. Mol. Biol. 196: 901–917, 1987.
7. Brummell, D.A., Sharma, V.P., Anand, N.N., Bilous, D., Dubuc, G., Michniewciz, J., MacKenzie, C.R., Sadowska, J., Sigurskjold, B.W., Sinnott, B., Young, N.M., Bundle, D.R., Narang, S.A. Probing the combining site of an anti-carbohydrate antibody by saturation mutagenesis: Role of the heavy chain CDR3 residues. Biochemistry 32:1180–1187, 1993.
8. Chien, N.A., Roberts, V.A., Giusti, A.M., Scharff, M.D., Getzoff, E.D. Significant structural and functional change of an antigen-binding site by a distant amino acid substitution: Proposal of a structural mechanism. Proc. Natl. Acad. Sci. U.S.A. 86:5532–5536, 1989.
9. Lavoie, T.B., Drohan, W.N., Smith-Gill, S.J. Experimental analysis by site-directed mutagenesis of somatic mutation effects on affinity and fine specificity in antibodies specific for lysozyme. J. Immunol. 148:503–513, 1992.
10. Schildbach, J.F., Near, R.I., Bruccoleri, R.E., Haber, E., Jeffrey, P.D., Novotny, J., Sheriff, S., Margolies, M.N. Modulation of antibody affinity by a non-contact residue. Protein Sci. 2:206–214, 1993.
11. Kelley, R.F. Determinants of antigen binding and anti-proliferative activity in a humanized anti-p185^{HER2} antibody. In: "The Third Annual IBC International Conference on Antibody Engineering." LoBuglio, A.F. (ed.). San Diego, CA: Internation Business Communications, 1992.
12. Glaser, S.M., Vasquez, M., Payne, P.W., Schneider, W.P. Dissection of the combining site in a humanized anti-Tac antibody. J. Immunol. 149:2607–2614, 1992.
13. Carter, P., Presta, L., Gorman, C.M., Ridgway, J.B.B., Henner, D., Wong, W.L.T., Rowland, A.M., Kotts, C., Carver, M.E., Shepard, H.M. Humanization of an anti-p185HER2 antibody for human cancer therapy. Proc. Natl. Acad. Sci. U.S.A. 89:4285–4289, 1992.
14. Shalaby, M.R., Shepard, H.M., Presta, L., Rodrigues, M., Beverley, P.C.L., Feldman, M., Carter, P. Development of humanized bispecific antibodies reactive with cytotoxic lymphocytes and tumor cells overexpressing the *HER2* protooncogene. J. Exp. Med. 175:217–225, 1992.
15. Kettleborough, C.A., Saldanha, J., Heath, V.J., Morrison, C.J., Bendig, M.M. Humanization of a mouse monoclonal antibody by CDR-grafting: the importance of framework residues on loop conformation. Protein Eng. 4:773–783, 1991.
16. Hildreth, J.E.K., August, J.T. The human lymphocyte function-associated (HLFA) antigen and a related macrophage differentiation antigen (HMac-1): Functional effects of subunit-specific monoclonal antibodies. J. Immunol. 134:3272–3280, 1985.
17. Hynes, R.O. Integrins: Versatility, modulation, and signaling in cell adhesion. Cell 69:11–25, 1992.
18. Rosen, H., Gordon, S. Current status review: adhesion molecules and myelomonocytic cell-endothelial interactions. Br. J. Exp. Pathol. 70:385–394, 1989.
19. Jones, P.T., Dear, P.H., Foote, J., Neuberger, M.S., Winter, G. Replacing the complementarity-determining regions in a human antibody with those from a mouse. Nature (London) 321:522–525, 1986.
20. Morrison, S.L., Johnson, M.J., Herzenberg, L.A., Oi, V.T. Chimeric human antibody molecules: Mouse antigen-binding domains with human constant region domains. Proc. Natl. Acad. Sci. U.S.A. 81:6851–6855, 1984.
21. Boulianne, G.L., Hozumi, N., Shulman, M.J. Production of functional chimaeric mouse/human antibody. Nature (London) 312:643–646, 1984.
22. Presta, L.G. Antibody engineering. Curr. Op. Struc. Biol. 2:593–596, 1992.
23. Kunkel, T.A., Roberts, J.D., Zakour, R.A. Rapid and efficient site-specific mutagenesis without phenotypic selection. Methods Enzymol. 154:367–382, 1987.
24. Carter, P., Kelley, R.F., Rodrigues, M.L., Snedecor, B., Covarrubias, M., Velligan, M.D., Wong, W.L.T., Rowland, A.M., Kotts, C.E., Carver, M.E., Yang, M., Bourell, J.H., Shepard, H.M., Henner, D. High level *Escherichia coli* expression and production of a bivalent humanized antibody fragment. Bio/Technology 10:163–167, 1992.

25. Munson, P.J., Rodbard, D. LIGAND: A computerized analysis of ligand binding data. Methods Enzymol. 92:543–576, 1983.
26. Scatchard, C. The attractions of proteins for small molecules and ions. Ann. N. Y. Acad. Sci. 51:660–672, 1949.
27. Messerschmidt, A., Pflugrath, J.W. Crystal orientation and X-ray pattern prediction routines for area-detector diffractometer systems in macromolecular crystallography. J. Appl. Crystallogr. 20:306–315, 1987.
28. Kabsch, W. Evaluation of single-crystal X-ray diffraction data from a position-sensitive detector. J. Appl. Crystallogr. 21:916–934, 1988.
29. Brünger, A. T. X-PLOR Reference Manual. Molecular Simulations, Inc., Waltham, MA, 1992.
30. Eigenbrot, C., Randal, M., Presta, L., Carter, P., Kossiakoff, A.A. X-ray Structures of the antigen-binding domains from three variants of humanized anti-p185^{HER2} antibody 4D5 and comparison with molecular modelling. J. Mol. Biol. 229:969–995, 1993.
31. Brünger, A.T. Extension of molecular replacement: A new search strategy based on patterson correlation refinement. Acta Crystallogr. Sect. A 46:46–57, 1990.
32. Brünger, A.T. Free R value: A novel statistical quantity for assessing the accuracy of crystal structures. Nature (London) 355:472–475, 1992.
33. Fujinaga, M., Read, R.J. Experiences with a new translation-function program. J. Appl. Crystallogr. 20:517–521, 1987.
34. Hodel, A., Kim, S.-H., Brünger, A.T. Model bias in macromolecular crystal structures. Acta Crystallogr. A48:851–858, 1992.
35. Brünger, A.T. Solution of a Fab (26–10)/digoxin complex by generalized molecular replacement. Acta Crystallogr A 47:195–204, 1991.
36. Fan, Z.-c., Shan, L., Guddat, L.W., He, X.-m., Gray, W.R., Raison, R.L., Edmundson, A.B. Three-dimensional structure of an Fv from a human IgM Immunoglobulin. J. Mol. Biol. 228:188–207, 1992.
37. Tulip, W.R., Varghese, J.N., Laver, W.G., Webster, R.G., Colman, P.M. Refined crystal structure of the influenza virus N9 neuraminidase-NC41 Fab complex. J. Mol. Biol. 227:122–148, 1992.
38. Davies, D.R., Sheriff, S., Padlan, E. Comparative study of two Fab-lysozyme crystal structures. Cold Spring Harbor Symp. Quant. Biol. 54:233–238, 1989.
39. Chothia, C., Lesk, A.M., Tramontano, A., Levitt, M., Smith-Gill, S.J., Air, G., Sheriff, S., Padlan, E.A., Davies, D., Tulip, W.R., Colman, P.M., Spinelli, S., Alzari, P.M., Poljak, R.J. Conformations of immunoglobulin hypervariable regions. Nature (London) 342:877–883, 1989.
40. Luzatti, V. Traitement statistique des erreurs dans la détermination des structures cristallines. Acta. Crystallogr. 5:802–810, 1952.
41. Weber, I.T. A vector-averaging method for locating small differences between nearly identical protein structures. J. Appl. Crystallogr. 20:388–393, 1987.
42. Kossiakoff, A.A., Randal, M., Guenot, J., Eigenbrot, C. Variability of conformations at crystal contacts in BPTI represent true low energy structures: correspondence among lattice packing and molecular dynamics structures. Proteins 14:65–74, 1992.
43. Eigenbrot, C., Randal, M., Kossiakoff, A.A. Structural effects induced by mutagenesis affected by crystal packing factors: The structure of a 30–51 disulfide mutant of basic pancreatic trypsin inhibitor. Proteins 14:75–87, 1992.
44. Rini, J.M., Schulze-Gahmen, U., Wilson, I.A. Structural evidence for induced-fit as a mechanism for antibody-antigen recognition. Science 255:959–965, 1992.
45. Herron, J.N., He, X.M., Ballard, D.W., Blier, P.R., Pace, P.E., Bothwell, A.L.M., Voss, E.W., Jr., Edmundson, A.B. An autoantibody to single-stranded DNA: Comparison of the three-dimensional structure of the unliganded Fab and a deoxynucleotide-Fab complex. Proteins 11:159–175, 1991.
46. Bhat, T.N., Bentley, G.A., Fischmann, T.O., Boulot, G., Poljak, R.J. Small rearrangements in structures of Fv and Fab fragments of antibody D1.3 on antigen binding. Nature (London) 34:483–485, 1990.
47. Bentley, G.A., Boulot, G., Riottot, M.M., Poljak, R.J. Three-dimensional structure of an idiotope-anti-idiotope complex. Nature (London) 348:254–257, 1990.
48. Kelley, R.F., O'Connell, M.P., Carter, P., Presta, L., Eigenbrot, C., Covarrubias, M., Snedecor, B., Bourell, J.H., Vetterlein, D. Antigen binding thermodynamics and antiproliferative effects of chimeric and humanized anti-p185HER2 antibody fragments. Biochemistry 31:5434–5441, 1992.
49. Lascombe, M.B., Alzari, P.M., Boulot, G., Saludjian, P., Tougard, P., Berek, C., Haba, S., Rosen, E.M., Nisonoff, A., Poljak, R.J. Three-dimensional structure of Fab R19.9, a monoclonal murine antibody specific for the p-azobenzenearsonate group. Proc. Natl. Acad. Sci. U.S.A. 86:607–611, 1989.
50. Colman, P.M., Laver, W.G., Varghese, J.N., Baker, A.T., Tulloch, P.A., Air, G.M., Webster, R.G. Three-dimensional structure of a complex of antibody with influenza virus neuraminidase. Nature (London) 326:358–363, 1987.
51. Rodrigues, M.L., Shalaby, M.R., Werther, W., Presta, L., Carter, P. Engineering a humanized bispecific F(ab')$_2$ fragment for improved binding to T cells. Int. J. Cancer: Suppl. 7:45–50, 1992.
52. Kelley, R.F., O'Connell, M.P., Carter, P., Presta, L., Eigenbrot, C., Covarrubias, M., Snedecor, B., Speckart, R., Blank, G., Vetterlein, D., Kotts, C. Characterization of humanized anti-p185^{HER2} antibody Fab fragments produced in *Escherichia coli*. In: Cleland, J.L., ed. Protein Folding In Vivo and In Vitro. Vol. 526. Washington, D.C.: American Chemical Society, 1993:218–239.
53. Presta, L.G., Lahr, S.J., Shields, R.L., Porter, J.P., Gorman, C.M., Fendly, B.M., Jardieu, P.M. Humanization of an antibody directed against IgE. J. Immunol. 151:2623–2632, 1993.
54. Eigenbrot, C., Randal, M., Kossiakoff, A.A. Structural effects induced by removal of a disulfide bridge: The X-ray structure of the C30A/C51A mutant of basic pancreatic trypsin inhibitor at 1.6 Å. Protein Eng. 3:591–598, 1990.
55. Housset, D., Kim, K.S., Fuchs, J., Woodward, C., Wlodawer, A. Crystal structure of a Y35G mutant of bovine pancreatic trypsin inhibitor. J. Mol. Biol. 220:757–770, 1991.